COR1 Engineering Test Unit Measurements at the NCAR/HAO Vacuum Tunnel Facility October–November 2002

William Thompson
December 6, 2002

1 Introduction

The Engineering Test Unit (ETU) of COR1 was made in two configurations. The first configuration, ETU-1, was for vibration testing, while the second, ETU-2, was for optical testing. This is a report on the optical testing performed on ETU-2 at the NCAR/HAO Vacuum Tunnel Facility during the months of October and November, 2002. This was the same facility used to test the two previous breadboard models.

In both configurations, the first two tube sections were complete, with all optical elements aligned. The vibration model ETU-1 had the remaining tube sections attached, with mass models for the remaining optics, for the various mechanisms, and for the focal plane assembly. It was then converted into the optical model ETU-2 by removing tube sections 3 to 5, and mounting the remaining optics on commercial mounts. (The bandpass filter was also installed into tube 2, which had been replaced in ETU-1 by a mass model, so that pre- and post-vibration optical measurements could be made.) Doublet 2 was installed in a Newport LP-2 carrier, and aligned to the other optics in the first two tube sections. The LP-2 adjustment screws were then uralened so that the alignment could be maintained during shipping.

Because neither the flight polarizer nor Hollow Core Motor were available, they were simulated by a commercial polarizer and rotational mount, both from Oriel corporation. The Oriel rotational stage was not designed for vacuum use, but it was determined after consultation with the company, and lab testing, that the stage could be used in the moderate vacuum conditions at the NCAR/HAO facility.

The shutter and focal plane assembly were simulated with the same camera used for the previous two breadboard tests. The focal plane mask was simulated with a plane of BK7 glass with a mask glued on, using the same procedure as for the Lyot spot on Doublet 1, and mounted in an adjustable LP-2 carrier. Two masks were made, one made to the precise specifications of the optical design, the other slightly bigger to make alignment easier.

2 Calibration

The calibration of the detector was established in the previous two breadboard tests. This was done by removing all the optics, and directly exposing the camera to the beam. By modeling how the beam is affected by the various optics and stops within the instrument, one can then predict what the signal on the detector should be if there were no occulter. The calibration from the previous two breadboards matched so closely, that it was decided that the optics removal procedure did not need to be repeated for the ETU.

However, several changes in the instrument and experimental setup need to be incorporated into the calibration procedure. First of all, the photodiode which was used to monitor the brightness of the beam was moved from the inner to the outer privacy screen. This was done because tube 1 of the ETU was slightly wider than in breadboard #2 (BB2). Instead of increasing the distance of the photodiode away from the optical axis, which may have affected the calibration, the diode was moved slightly forward at the same transverse position. Since the beam is collimated, this motion purely along the optical axis does not affect the calibration.

It was discovered that the source iris was slightly undersized in the previous two breadboard measurements. This was because of a misunderstanding of the size of the occulter, and a failure to take into account the extra distance between the guiding ring and the actual aperture position. For the ETU tests, the iris diameter was increased from 9.765 inches to the correct 10.702 inches.

Other factors which affect the calibration are the reduction of the Lyot stop from 34 mm to 30 mm, and the reduction of the plate scale from 6.71 arcsec/pixel for BB2 to the design value of 5.81 arcsec/pixel for the ETU. When all these factors are taken into account, the calibration is changed by a factor of 0.478 from that of BB2. We will use this as a provisional calibration, until a complete analysis of the ETU optical design is completed, including the effect of the AR coatings.

We also took with us a 4.0D neutral density filter. By inserting this filter in the optical path, we can cut down the intensity of the light sufficiently to come within the capabilities of the camera. This procedure is used only as a check on the calibration, because the accuracy and uniformity of the neutral density filter is not known, and because the source image cannot be placed completely within the field of view. Figure 1 shows an image of the source iris taken through the ND filter, along with a trace through the image, adjusted by 10^4 to take the filter into account. This shows that the data is very close to the expected value of 1. The bulk of the data lies somewhat above 1, but this may be caused by the transmission of the ND filter being slightly different than 10^{-4} at 700 nm. Given the constraints of the test, it was a highly successful confirmation of the calibration technique.

Another property that can be derived from Figure 1 is the plate scale. Measurements of the image edge show that it is a circle with a radius of 178.2 pixels. The source iris, at a distance of 1155 inches, and a diameter of 10.702 inches, subtends 1911 arcseconds. Thus, the plate scale must be 5.36 arcsec/pixel, which is smaller than the expected 5.81 arcsec/pixel. For that and other reasons, the current calibration should only be considered provisional.

3 Resolution

To test the resolution of the ETU, a target was placed at the iris location, and the instrument off-pointed so that the target could be imaged. A standard Air Force 1951 resolution test target was used, downloaded as a PDF image off the internet, and printed as a transparency on a high-resolution 600 dpi printer. To keep the light levels within the capability of the camera, only ambient light was used to illuminate the target—the solar tracking mirrors were not used.

First, the best focus position of the camera had to be established. It was not possible to establish the optimal focus position for the camera during assembly, because the relationship between the CCD surface and the outer body of the camera was not known. Instead, the camera was moved through a range of positions to find the location where the source image was sharpest. A ruler was used to measure the distance between the back of the camera stage and a fiducial along the

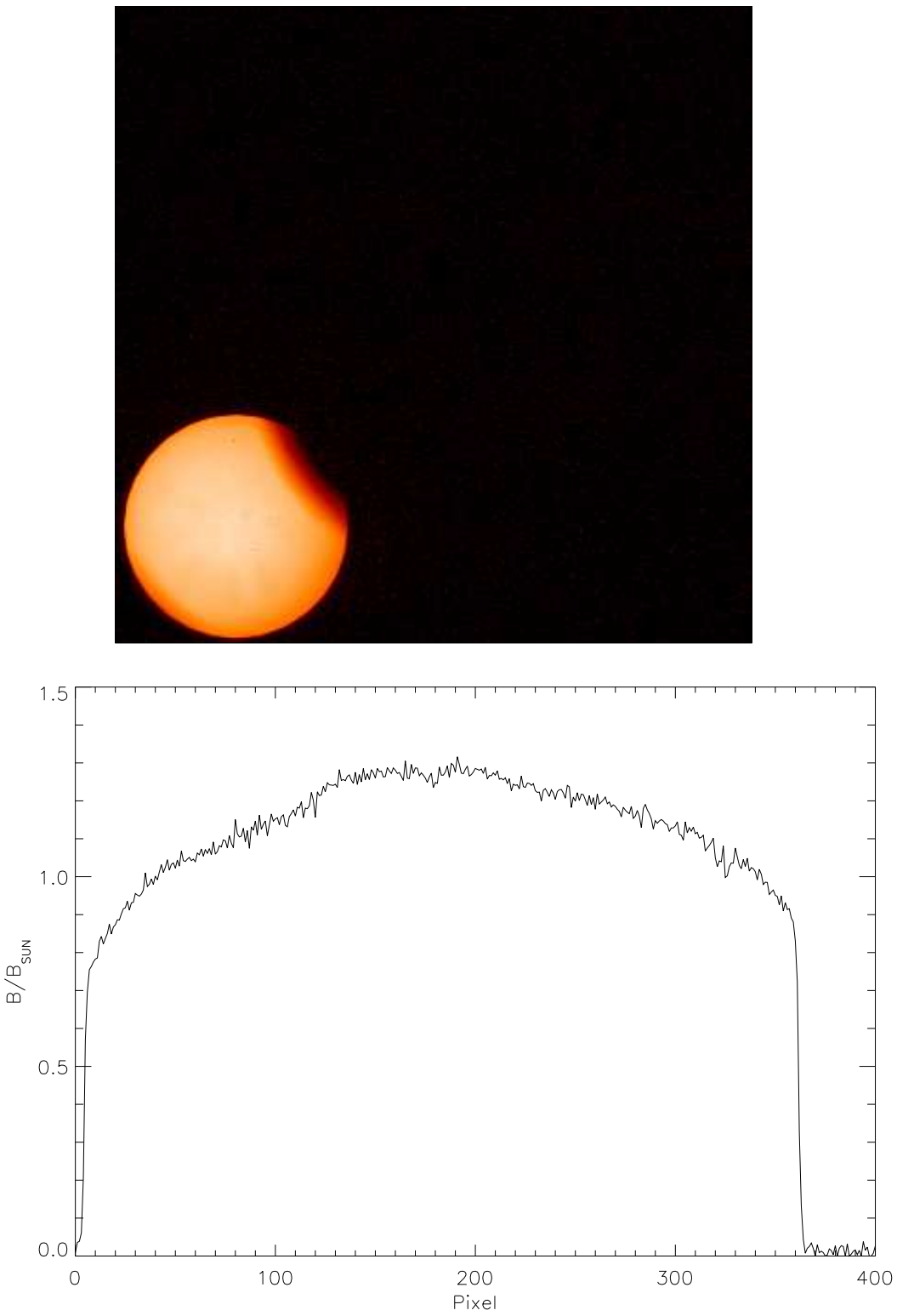

Figure 1: Top: image of the source iris taken through a 4.0D neutral density filter. Bottom: vertical trace of the source intensity, boosted by 10^4 to adjust for the neutral density filter.

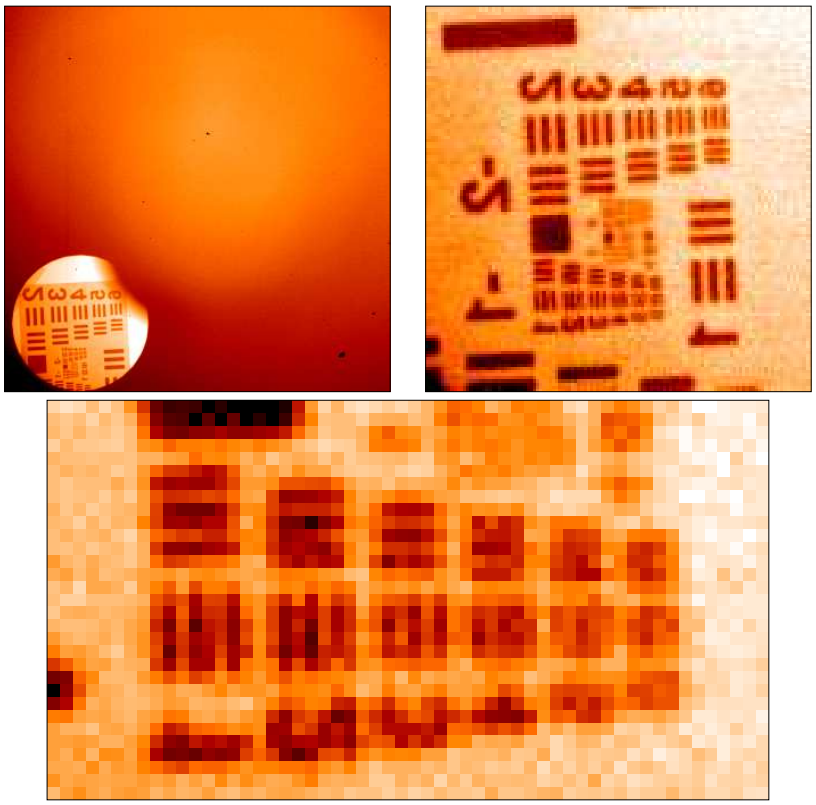

Figure 2: Images of the Air Force resolution test target, at various magnifications.

rail. Measurements were always made along the right side of the rail. The original fiducial was the end of the rail itself, and the initial focusing based only on the edge of the iris put the optimal camera position at 479 mm from the end of the rail. For the more sensitive requirements of the focusing test, a piece of kapton tape was placed near the back end of the rail, and measurements were made from the back end of the kapton to the base of the camera stage. From this fiducial, the initial position was equivalent to 452 mm. Images of the Air Force target were made with camera positions from 454 mm to 450 mm, stepping by half-millimeter increments. This was enough of a range to clearly show that it contained the point of best focus, which was found to be at 451.5 mm, although it was difficult to tell this apart from 452 mm.

Figure 2 shows images of the resolution test target at the 451.5 mm focus position, at various magnifications. The highest magnification image shows clearly that bars can be imaged which are separated by only one pixel, i.e. at the Nyquist frequency. In particular, look at group (-1,3) which appears to be the closest to the Nyquist frequency.

4 Stray light

The scattered light properties of the ETU were measured using the same procedure as for the two previous breadboards. The initial measurements were made without the polarizer or focal plane mask, which were added in later in separate tests.

Unlike the ultimate flight units, the ETU as delivered to NCAR/HAO was open in the back,

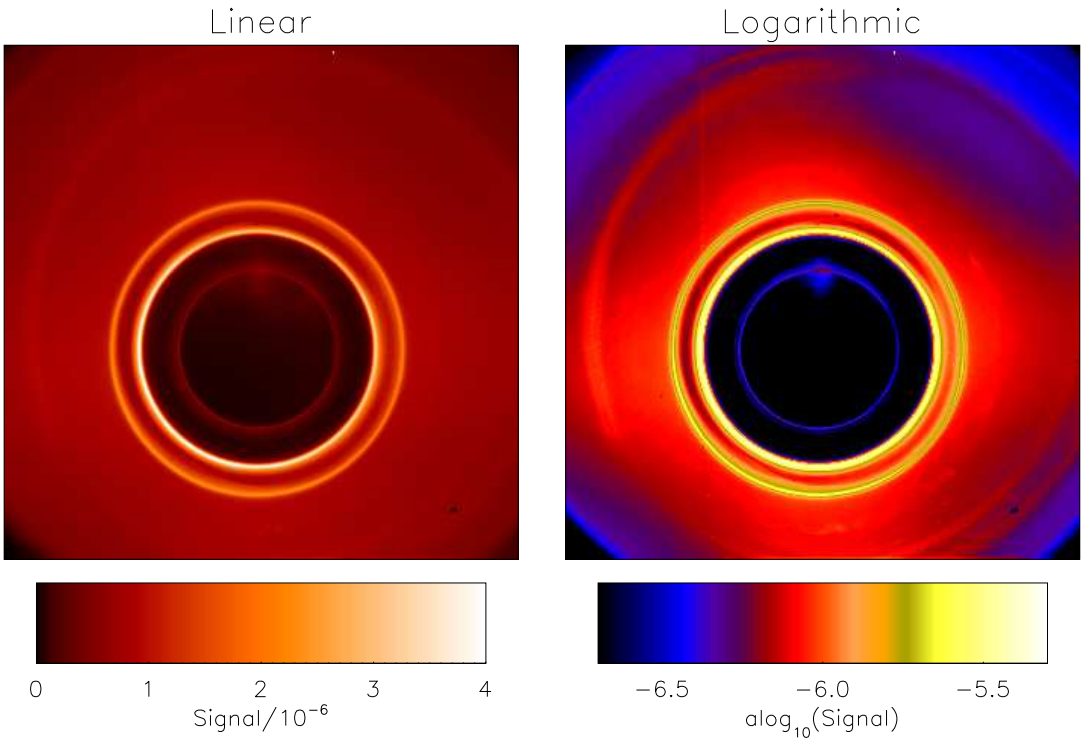

Figure 3: Scattered light pattern from objective #1, in both linear and logarithmic presentations.

with no baffling past Doublet 1. It was found that this resulted in anomalous stray light hitting the detector, so an extemporaneous baffling system was devised by Les Putnam, using black tape and llumalloy, which successfully removed the anomalous stray light.

Alignment was established by tilting the instrument in both pitch and yaw until the source peeked over the occulter edge on either side. The midpoint between positions where the source just peeked over was taken as the optimal alignment. The camera was placed where the source was in best focus, as discussed in Section 3. The occulter itself was slightly out of focus, as called for in the optical design.

The measured scattered light pattern is shown in Figure 3. The behavior is very similar to that seen in BB2. Two bright rings surround the occulter shadow, which were shown in previous tests to mark the edges of the umbra and penumbra. A third fainter ring appears within the occulter shadow. The scattered light pattern outside the occulter is marked by four faint rays radiating outward from the source image behind the occulter. Similar rays were seen in BB2, but in different directions, and were identified with the cleanliness of the objective lens. There are also a number of arcs in the image. One way to explore the source of features within the image is to rock the instrument pointing from side to side, and look at how the features respond. Features such as the rays follow the motion of the source, as do a few of the fainter arcs. The brighter arcs, however, do not move, suggesting that they may be related to the structures within the instrument structure. Since the structures past tube section # are not flight-like, these non-flight structures may be responsible for the arcs. For example, the shutter housing in the breadboard camera could easily create arcs such as these.

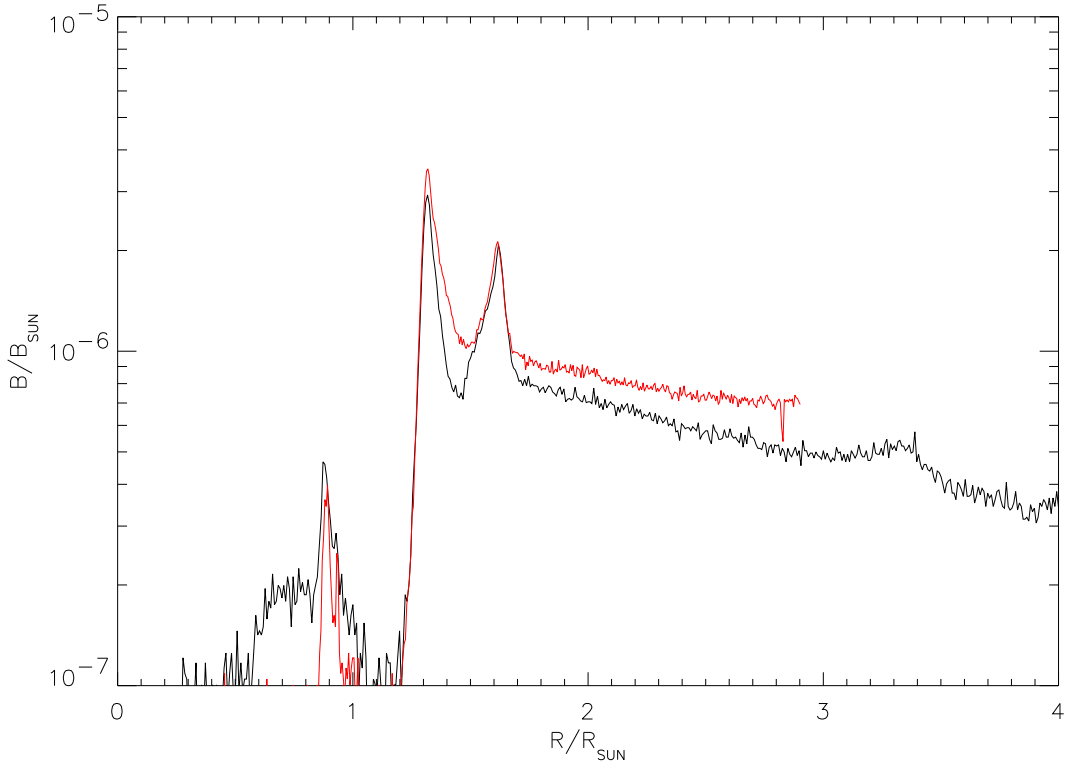

Figure 4: Traces of the scattered light pattern from Figure 3. The black trace is made at a 45° angle from the center of the pattern towards the upper right corner. The red trace is a horizontal trace from the center towards the right edge.

Figure 4 shows the same data as in Figure 3, in graphical form. The black curve shows a trace of the data at a 45° angle from the occulter center towards the upper right corner, avoiding the rays of enhanced scattering. The performance is similar to that of BB2, with levels just under 10^{-6} near the occulter edge, declining to about 3×10^{-7} at 4 solar radii. The red curve shows a horizontal trace from the center to the right edge, along one of the rays of increased scattering. In general, the ETU performance ranges from being similar to that of BB2, to being somewhat better.

It should be noted that the bright rings around the edge of the occulter are substantially reduced from those of BB2, by about a factor of 5. This was accomplished by reducing the Lyot stop size from 34 mm to 30 mm. Measurements made with BB2 after the last NCAR/HAO test predicted almost precisely this level of improvement, and the ETU tests bear it out.

5 Field of view

The COR1 requirements call for an unobstructed field of view out to ±85° from the center of the objective, to avoid unwarrented stray light entering the instrument. However, several spacecraft features may poke slightly into that keep-out zone. In particular, one of the separator springs will poke in by about 1 inch at a distance of 12 inches. Thus, it was decided to test the sensitivity of the instrument to scattering sources well outside the detector field of view, but inside the unobstructed

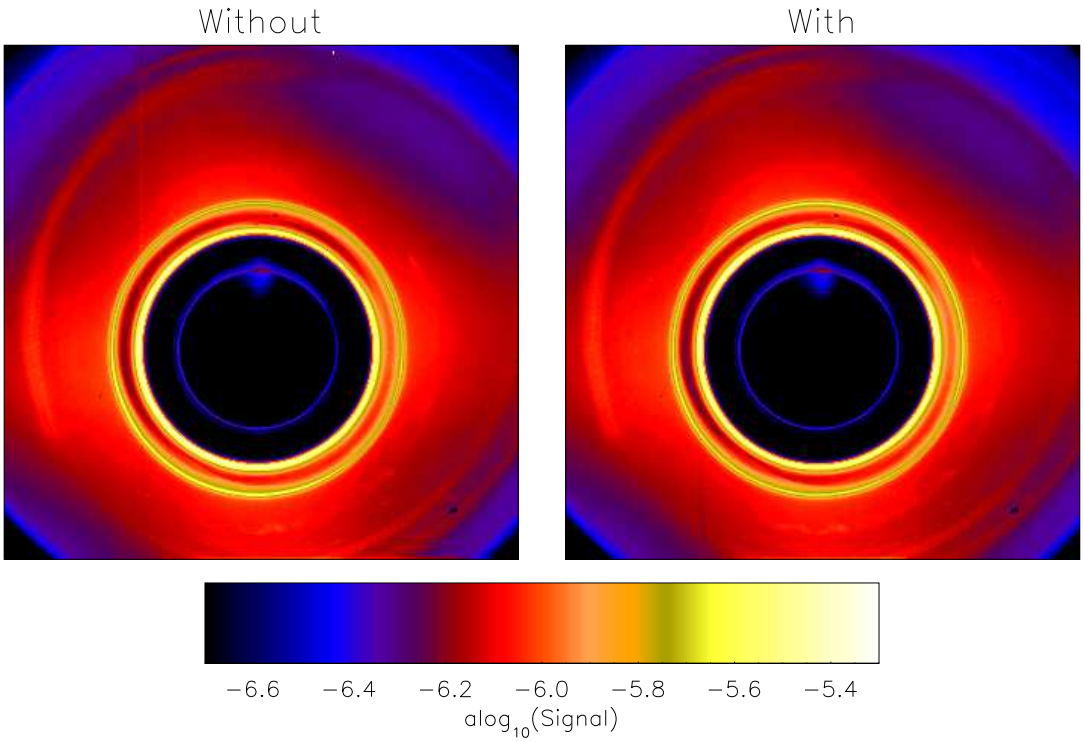

Figure 5: Comparison of images made with and without a scatterer to the side of the field of view.

field of view requirement.

To test this, we placed a shiny spring in the beam to the side of the objective. The spring was about 4 cm long, with its center about 4 cm in front of the objective. The radial distance from the center of the objective was about 7.2 cm. Therefore, this scatterer subtended angles approximately $42° - -74°$ off from the optical axis, and thus posed a much more stringent challenge to COR1 than anything that will be seen on the spacecraft. The results are shown in Figure 5—the images with and without the spring are indistinguishable.

6 Polarization

As part of the test, a commercial linear polarizer was introduced into the optical path to simulate the polarizer that will be used in flight. A rotational stage was used to control the polarizer while under vacuum. By taking images at several polarizer positions, the state of polarization of the signal can be determined.

The signal I for a given polarizer angle ϕ can be expressed as

$$I(\phi) = \frac{1}{2} I_u + I_p \cos^2(\theta - \phi) \tag{1}$$

where θ is the angle of polarization, and I_u and I_p are the unpolarized and polarized components

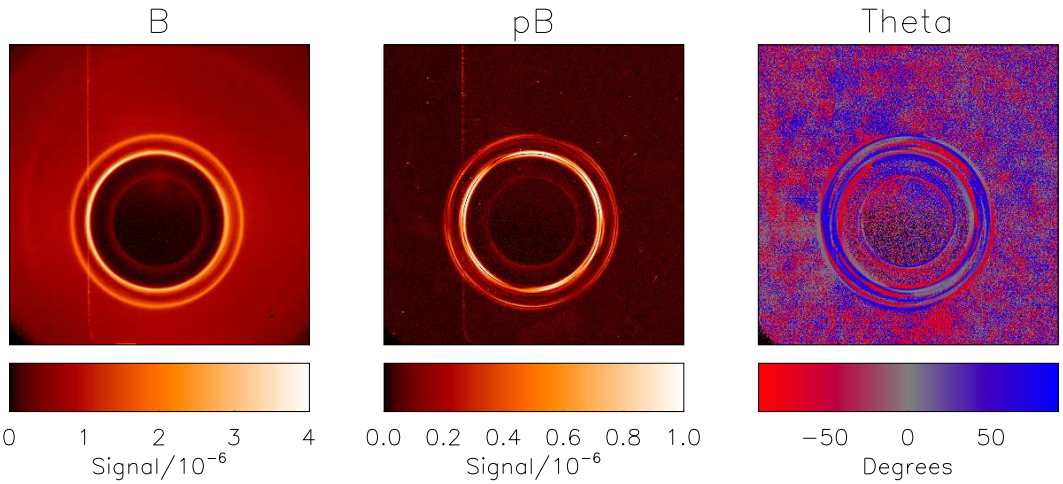

Figure 6: Total (B) and polarized (pB) brightness images, and a map of the polarization phase angle (θ).

respectively.[1] (A common notation is to use $B = I_u + I_p$ for the total brightness, and $pB = I_p$ for the polarized brightness.) If one takes three images I_a, I_b, I_c with polarizer angles either 60° or 120° apart, then the polarized brightness can be derived as

$$pB = I_p = \frac{4}{3}\sqrt{(I_a + I_b + I_c)^2 - 3(I_a I_b + I_a I_c + I_b I_c)} \tag{2}$$

while the total brightness is simply

$$B = I_u + I_p = \frac{2}{3}(I_a + I_b + I_c) \tag{3}$$

Figure 6 shows the result of applying Equations 2 and 3 to ETU data. A strong polarization signal is seen in the bright rings at the edge of the occulter, with little or no polarization signal seen elsewhere.

One has to be aware of the fact that noise in the data can induce a spurious polarization signal. The essence of Eq. 2 is to look for differences between images, and noise will induce differences in otherwise identical images. The mathematics behind Eq. 2 is to solve three equations of the form Eq. 1 in the three unknowns I_u, I_p, and θ. Note that Eq. 2 will always return a positive number for I_p. Thus, given that measured signals will always have some noise in them, there will always be an apparent polarized signal in the data. The ETU data are particular subject to this effect, because the source brightness at the NCAR/HAO facility is several orders of magnitude fainter than the Sun. Even with the 300 second integration times that were used for the data in Figure 6, one is still underexposing by about 2 orders of magnitude compared to what is expected for flight.

There are several ways to beat down the noise to improve the polarization measurement. One way is to do pixel averaging. For the ETU data, it was decided to average together in blocks of 9×9 pixels. Hence, the total number of photons collected into these binned pixels should approximate the expected number in flight. (The data shown in Figure 6 was only binned by a factor of 3×3,

[1] An additional factor of 0.77 is applied to the calibration when the polarizer is in place. This factor was derived from intercomparing data with and without the polarizer, and is consistent with the typical transmission curve given on the Oriel web site.

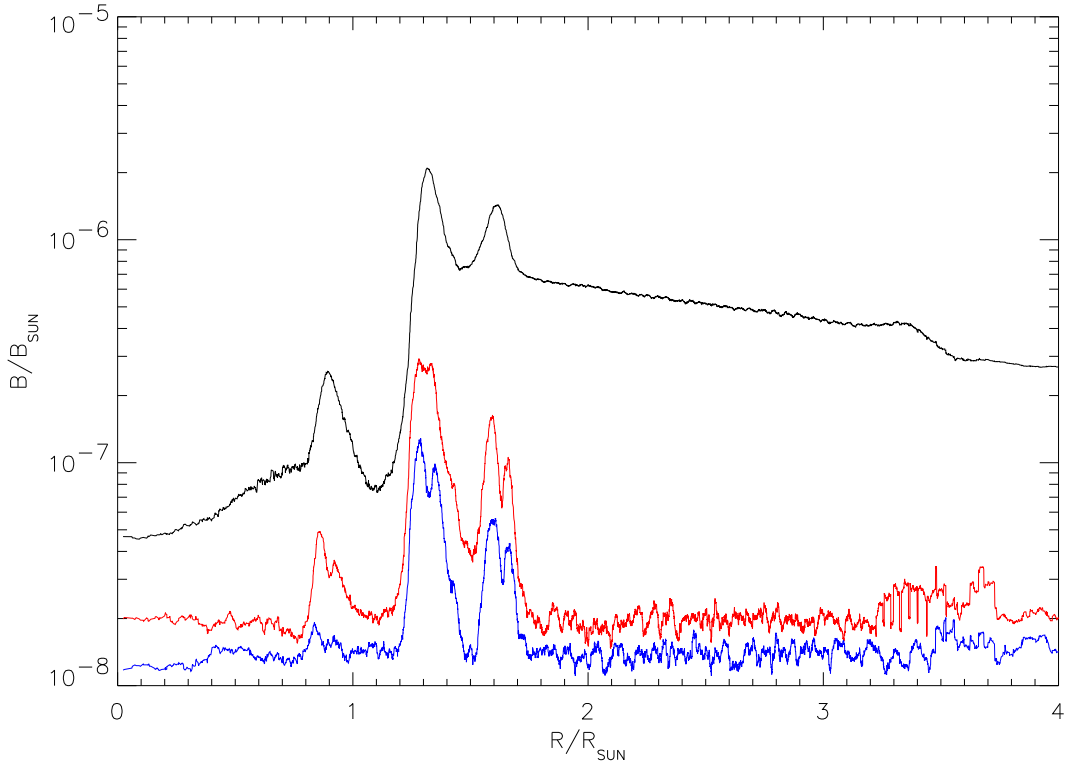

Figure 7: Brightness and polarized brightness as a function of radial position. Black: total brightness (B). Red: fitted polarized brightness (pB). Blue: fitted polarized brightness with images analyzed in random order.

to show the finer scale features, and thus is noisier.) Another way to beat down the noise is to measure at a larger number of angles. To this end, we took a series of measurements with the polarizer moved in 10° increments from 0° to 180°, plus the angles 45° and 135°. The resulting series of 21 images can then be approached as a least-squares fit at each pixel to Eq. 1.

Figure 7 shows the result of this procedure, showing the average behavior as a function of radial position. The left side of each image was masked off from this analysis, to avoid known problems with that part of the detector. The total brightness is plotted in black, and the fitted polarized brightness is in red. We then repeated the analysis with the images randomly shuffled, to help determine how much of the measured polarization signal is noise induced. The polarized brightness from this "control case" is plotted in blue in Figure 7.

It's evident from Figures 6 and 7 that the bright rings around the occulter edge are strongly polarized, with fractional polarizations on the order of 10–20%. Beyond the occulter, the fitted polarization signal hovers around $2 \times 10^{-8} B_\odot$, which can be compared to $\sim 1.4 \times 10^{-8} B_\odot$ for the control case. Although these numbers are close, there is a clear distinction between the two cases. Therefore, one concludes that the fitted polarized brightness is real, and that there is a 1–2% residual polarization signal in the diffuse scattering component. To further demonstrate that this is a real effect, and not just a numerical fluke, Figure 8 shows the relative brightness as a function of polarizer angle, averaged over a fairly large area on the right side of the image, where the breadboard detector characteristics are most stable. The sinusoidal variation with an amplitude of

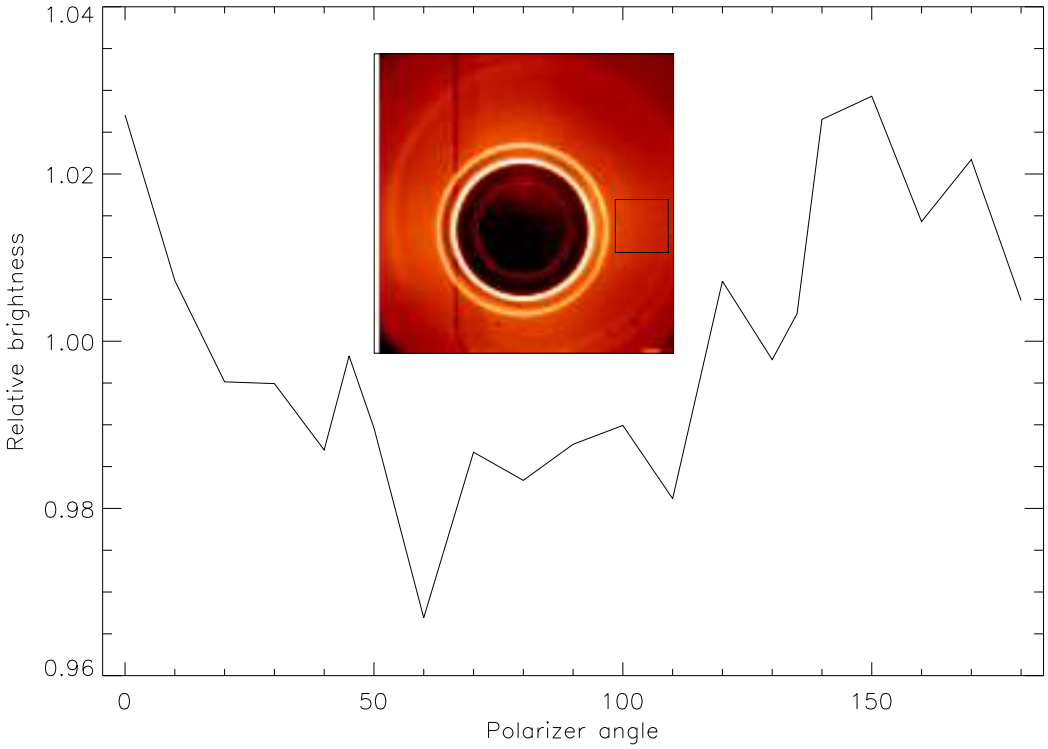

Figure 8: Relative brightness as a function of polarizer angle, for an area of 189×189 pixels to the right of the bright rings. The inset shows the location of the analyzed data.

∼2% is unmistakable.

6.1 Phase angle

As well as the polarized brightness, it is also possible to extract the polarization phase angle θ. A map of the phase angle measured with the ETU is shown in Figure 6. The rings stand out quite clearly from the noise. The actual polarization state of the rings is quite complex. One would expect the phase angle to rotate 360° as one makes a circle around the optical axis, and this is indeed the case. However, the phase also rapidly rotates through 90° going from the interior to exterior of each ring, and that was unexpected.

The phase angle situation outside of the rings is not clear from Figure 6, which was calculated with only a modest binning of 3×3 pixels. Analysis with a much more aggressive binning of 31×31 pixels shows that the phase angle outside of the rings does appear to show coherence over large areas, and to rotate roughly as expected as one goes around the optical axis. However, this analysis could only be done on the right side of the detector, where the breadboard detector characteristics are most stable. Where it could be reliably determined, the angle of polarization outside of the rings was found to be parallel to the radial vector. This is in contrast to the expected polarization from the corona, which should be transverse to the radial vector.

6.2 Observing a polarized source

To test the ability of the instrument to measure an intrinsically polarized signal, a sheet polarizer was placed in the beam in front of the ETU objective, by taping it to the sensor ring for the solar tracking system. Not only did this polarize the light entering the instrument, but it also created a large scattered light signal which overwhelmed the instrument's own scattered light profile. The measured polarized brightness, using Eq. 2, was ∼99% of the total brightness, close to the expected value of 100%. The phase angle of this measured polarized signal was fairly constant over the image at ∼5°, which presumably represents the relative alignment of the sheet polarizer to the instrument.

7 Focal plane mask

Two focal plane masks were delivered with the instrument, one with a diameter made to the precise specification of the optical design, and the other about 10% larger to make alignment easier. These masks were only provisionally aligned before the ETU was shipped to Colorado. The final alignment was to be done with the instrument in the NCAR/HAO chamber. Alignment in the directions perpendicular to the optical axis was controlled with two knobs on the side and top of the LP2 holder. There was also a lever on the LP2 for moving the mask along the optical axis. In addition, the whole carrier could be moved along the rail.

In order to fit the focal plane mask and its LP2 holder onto the rail, the camera needed to be moved back along the rail. When the mask holder was placed in its default position, which had been marked before shipment with a piece of kapton tape, and the camera moved as close to the mask as possible, the camera was at position 423.5 mm, or 28.5 mm closer to the end of the rail than was used for the other tests.

The task of aligning the focal plane mask so that the rings were completely obscured turned out to be much harder than originally thought. In the end, to quicken the process, we decided to concentrate only on the larger mask. We were able to correctly align this mask, but only by moving it substantially along the rail towards the back, and by moving the lever on the LP2 all the way over to place the mask as close to the camera as possible. The final position of the camera was 418 mm, so the mask had to be placed 5.5 mm further along the rail than originally anticipated, plus whatever distance is due to the lever. The total distance was about 8 mm. Most likely, the smaller properly sized mask would have had to be moved even further back from the expected position.

Even though the mask had to be located at a position different from that anticipated, the intended action of obscuring the rings around the occulter edge was highly successful, as shown in Figure 9. These data were taken in air, with the camera warm, so the images are noisier than most of the other data presented here. There's evidence that the introduction of the mask adds some additional scattering on the order of $10^{-7}B_{\odot}$, but the configuration of the mask to detector interface is so much different from that which will be used for flight that the significance of this small added scattering is unclear.

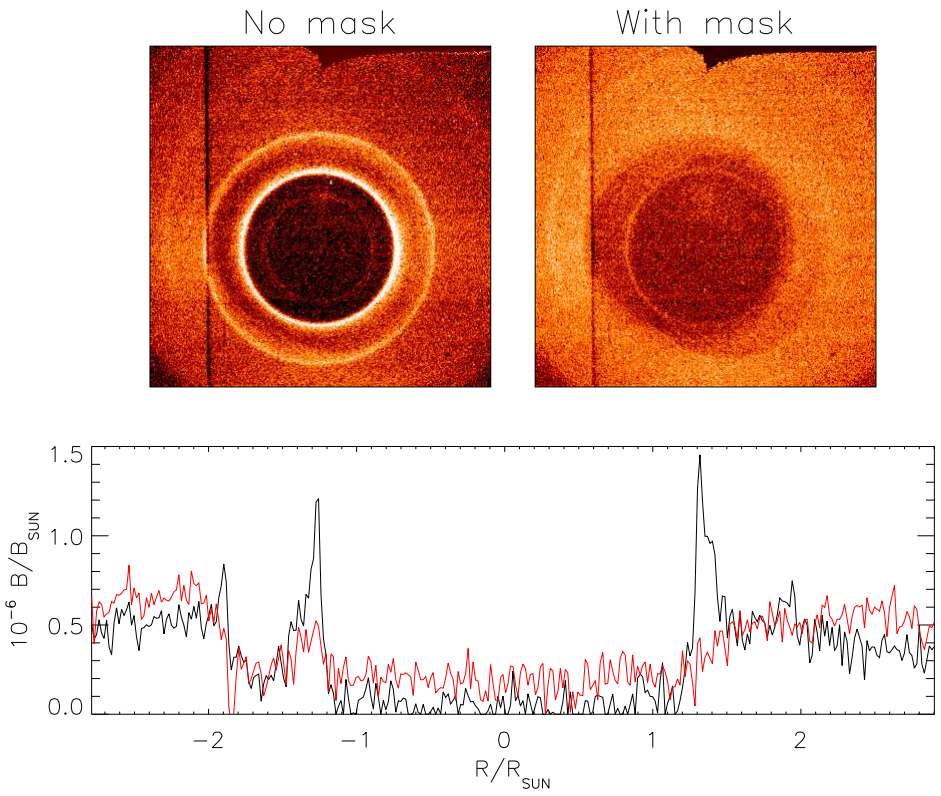

Figure 9: Comparison of images made with and without a focal plane mask. The graph shows vertical traces through the centers of each image.

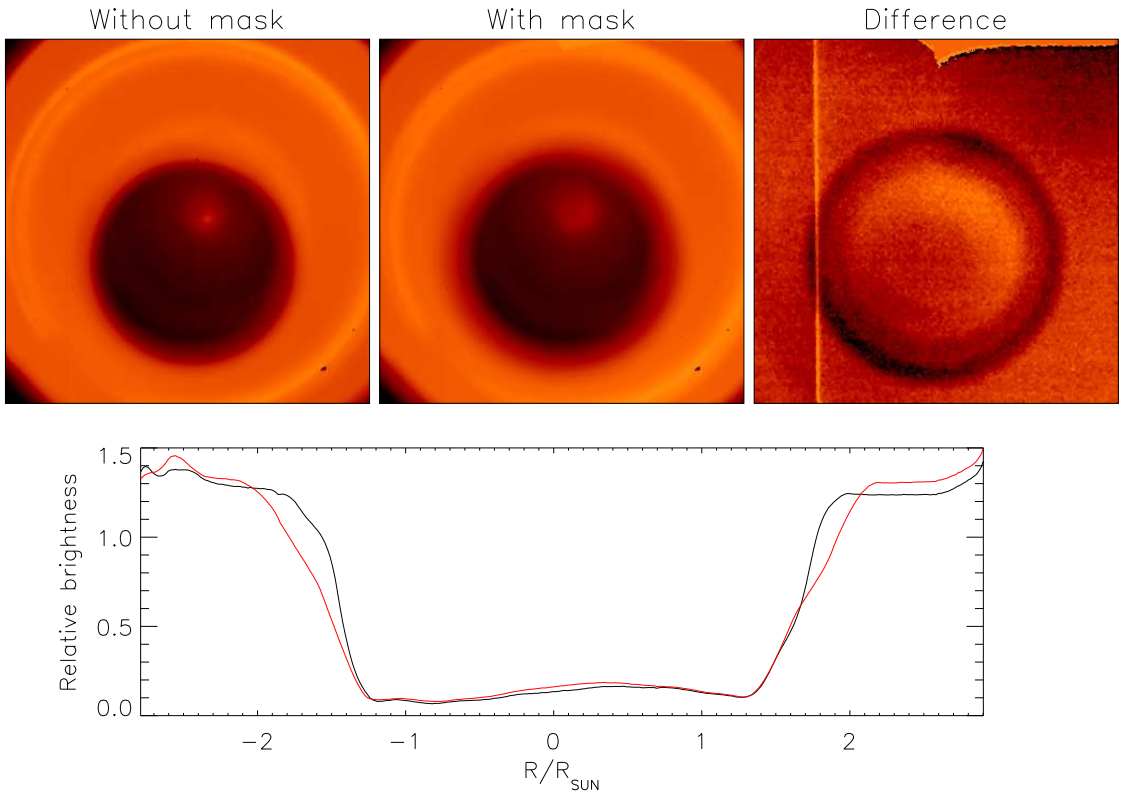

Figure 10: Images taken with a diffuser placed in front of the objective lens. The left and middle images are without and with the focal plane mask, respectively, and the rightmost image is the difference between the two cases. The bottom graph is a horizontal trace through the center of the occulter for the two cases, in arbitrary units. See the text for a fuller explanation of this figure.

8 Diffuser

The COR1 flight instrument will have a diffuser mounted in the door just in front of the objective. The purpose of this diffuser is to be able to stimulate the instrument while the door is closed, and to provide a source for flat-fielding and calibration purposes. To simulate this diffuser, a flashed opal diffuser was placed on an optical stand directly in front of the objective.

Figure 10 shows images taken with this diffuser in place, for cases with and without the focal plane mask. Some explanation is required for this figure. We took two approaches to illuminate the diffuser. One approach was to simply shine a flashlight on the diffuser, which provided a strong but uncalibrated signal. The other approach was to use the beam coming down the tunnel, which was much weaker, but which could be calibrated. Since the camera baffling was removed for these tests, to facilitate the various changes, there was some additional scattered light on the detector, which mostly affected the fainter images taken with the beam from the tunnel. Therefore, for clarity, the two images marked as "Without mask" and "With mask" on Figure 10 are those taken with the flashlight illumination, as is the graph. The difference image, on the other hand, is from the calibrated data, since the additional scattered light cancels out in the subtraction. For all of these data, the camera was displaced backwards to a position of 418 mm to make room for the focal plane mask.

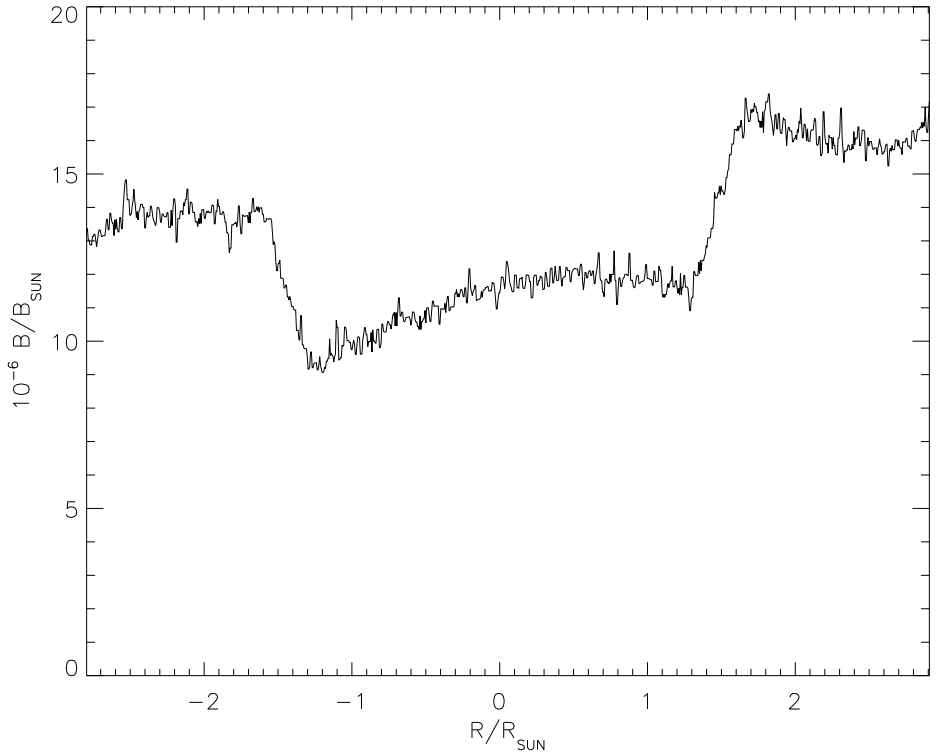

Figure 11: Horizontal trace through an image taken with the diffuser. See the text for a fuller explanation.

The diffuser used for the above tests had a measured BTDF of 0.14 sr^{-1} at normal incidence. The source had a diameter of 10.702 inches at a distance of 1155 inches, and therefore subtended 6.74×10^{-5} sr. The difference in radiance between the direct source and the diffused source should then be $0.14 * 6.74 \times 10^{-5} = 9.44 \times 10^{-6}$. Figure 11 shows the measured radiance coming from the diffuser, this time with the camera at position 452 mm, where the source is in focus. Comparison of Figure 11 and Figure 10 makes evident the extra stray light that was present in the calibrated data. However, looking solely at the contrast between the occulted and unocculted areas, a brightness of $\sim 5 \times 10^{-6} B_{\odot}$ can be derived, a factor of two lower than predicted.

It's not clear what caused this factor of two discrepancy between the diffuser measurements and the theoretical results. The only clue that we have is in the brightness measured for the rings around the edge of the occulter. The diffuser measurements were made on the 13th of November. On the 12th, with objective #2, the ring brightness was consistent with Figure 4. Objective #1 was then restored, and the diffuser measurements were made on the 13th. The next time the ring brightness could be checked directly against Figure 4 was on the 14th, when the test was made of moving the camera along the rail. (See Section 10.) At that time, the rings were only half the brightness they were before. The ring brightnesses were also low during the final focal plane mask tests (Figure 9), which were made late on the 12th. It may be that something happened between Nov 12 and Nov 14 which changed the instrument calibration by a factor of two. One possibility is that the polarizer was mistakenly put into the optical path without being recorded. There was some discussion on the 12th of putting in the polarizer while objective #2 was still in place, but it

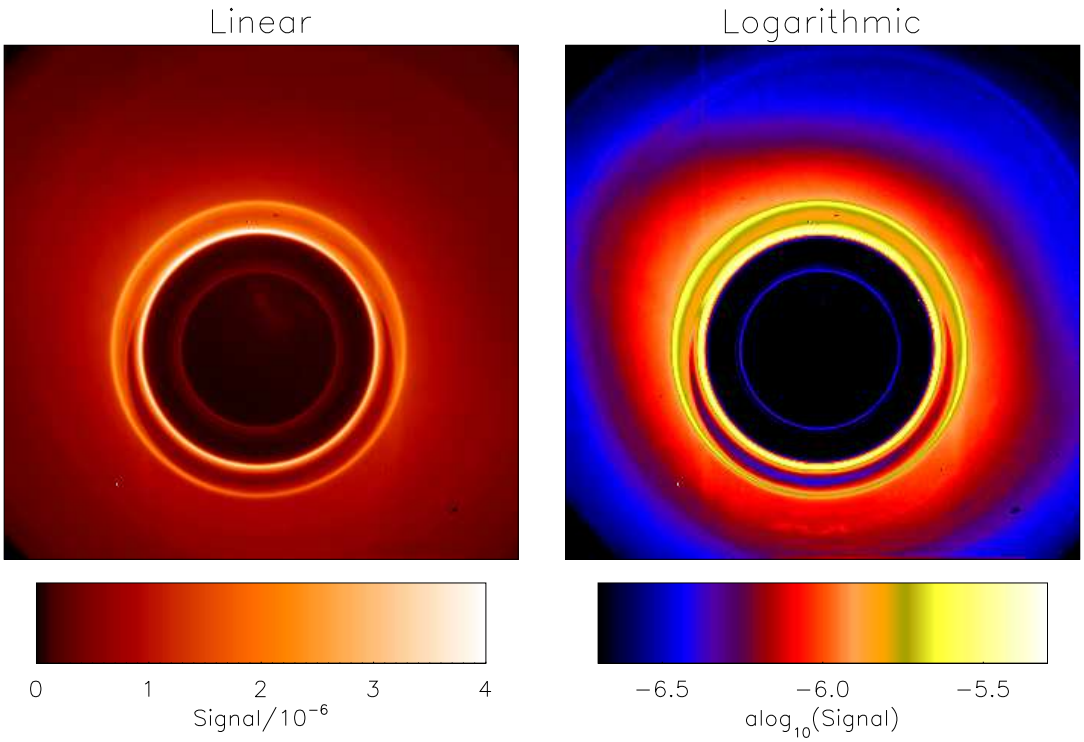

Figure 12: Scattered light pattern from objective #2, in the same presentation as in Figure 3.

was decided to forge ahead with the focal plane mask tests instead. If the polarizer was in place, then the corrected diffuser signal would be $\sim 1.3 \times 10^{-5} B_{\odot}$.

9 Objective lens changeout

Part of the plan for the COR1 instrument is to have a pre-aligned spare objective which can be switched out in case the original objective becomes contaminated. The procedure for changing out the objective was tested during the NCAR/HAO tests. Figure 12 shows the scatter pattern for the second objective. Instead of the four rays at the compass points seen with objective #1, one sees only two rays along a diagonal going from upper left to lower right. There also appears to be extra light between the two rings in the upper half of the image, and less light in the corresponding area in the lower half, when compared to objective #1. The average behavior with radial distance of the two lenses is compared in Figure 13. On the whole, objective #2 has somewhat more scattered light close to the occulter, and somewhat less scattered light at large distances.

The resolution of the second objective was tested by off-pointing to move the source image off the occulter. The edge of the source image was found to be just as sharp as that seen with objective #1.

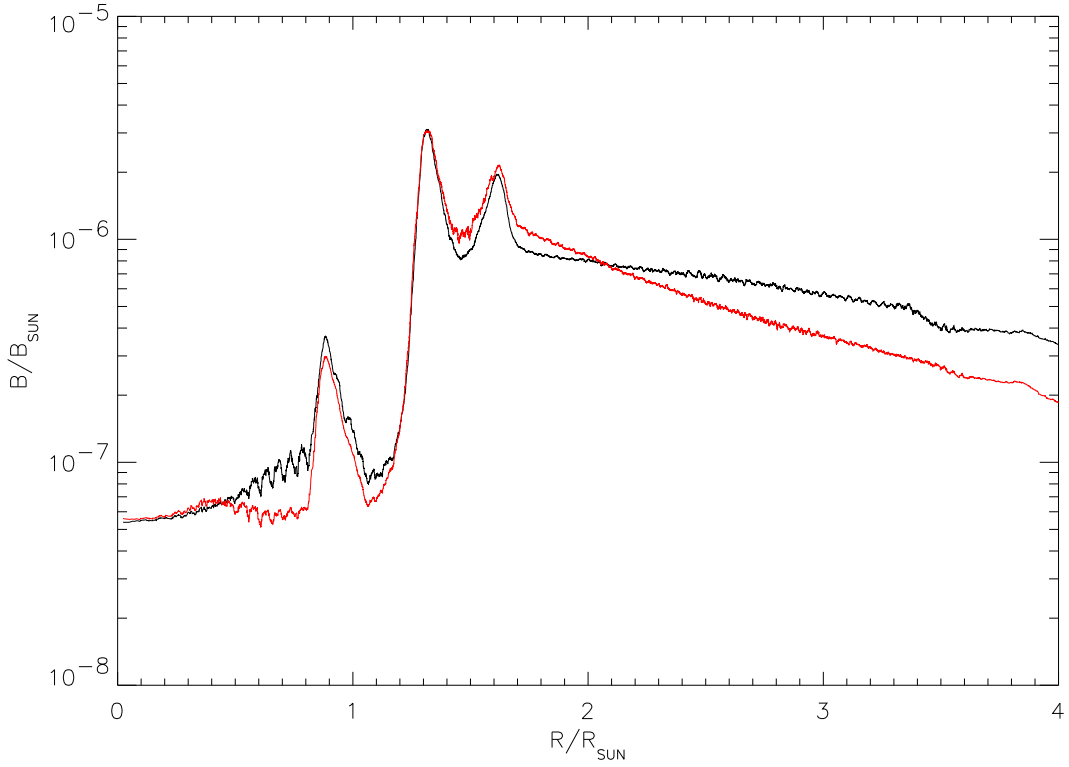

Figure 13: Comparison of average stray light from the two objectives, as a function of radial distance. Objective #1 is shown in black, and objective #2 is shown in red.

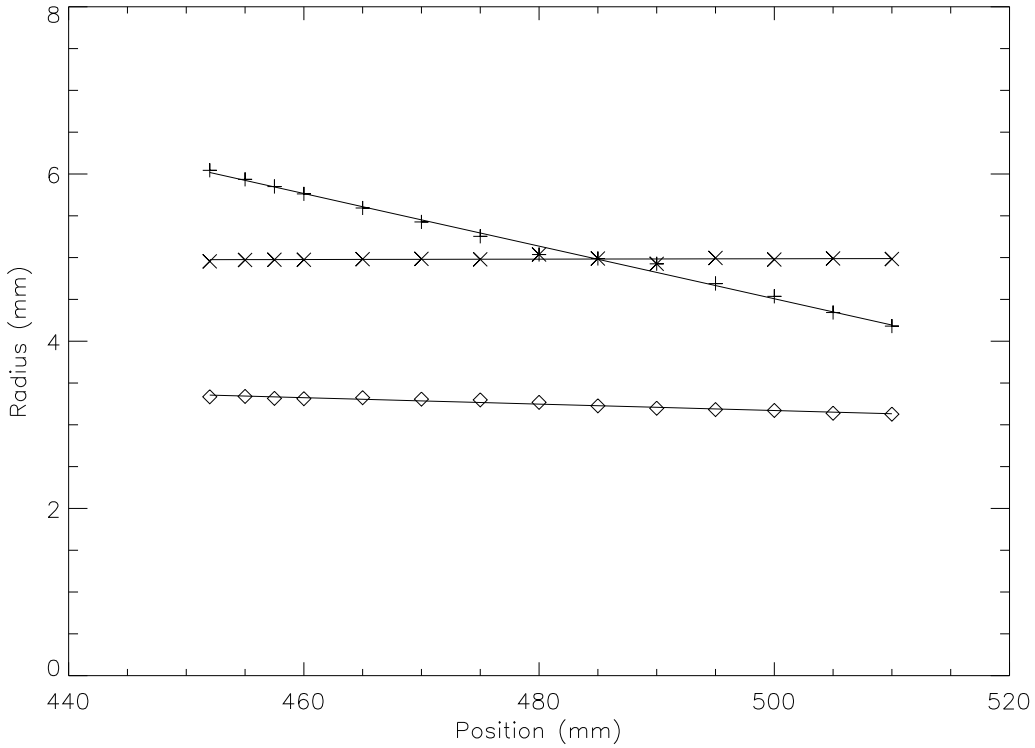

Figure 14: Radii of circles seen in the image as a function of camera postion. The intersection of the upper two curves marks the location where the occulter comes into focus. The leftmost data marks where the source is in focus, at 452 mm.

10 Ring profile along rail

To determine the behavior of the bright rings along the optical path, a series of images were taken with the camera at different positions along the rail, starting with the position where the source is in focus at 452 mm, and moving through the occulter focus. The radius of each of the rings was then measured at each position. The results are shown in Figure 14. It was previously determined that the two outer bright rings mark the edges of the umbra and penumbra of the occulter shadow. Therefore, the two rings merge when the occulter comes into focus. This occurs at 485 mm, which is about 33 mm in front of where the source is in focus. The radius of the focused occulter image is 4.983 mm.

The source of the faint ring within the occulter shadow is not known. It intersects with the outermost ring at a location about 96–97 mm in front of the source focus, where both rings have a radius of 2.98 mm. A detailed examination of this faint innermost ring shows that it's made up of two narrow rings, and a fainter broader ring. One possible explanation is that it is a some kind of ghost image.

NVTF/ML-074 Cleanroom - Verification of ISO 14644-1, Class 7 (FED-STD-209E Class 10,000) Compliance

ISO 14644-1 AIRBORNE PARTICULATE CLEANLINESS CLASSES

Cleanliness class designations and quantity have changed from FED-STD-209E. ISO 14644-1 adds three additional classes - two cleaner than Class 10 and one dirtier than Class 100,000.

	Number of Particles per Cubic Meter by Micrometer Size					
CLASS	0.1 µm	0.2 µm	0.3 µm	0.5 µm	1 µm	5 µm
ISO 1	10	2				
ISO 2	100	24	10	4		
ISO 3	1,000	237	102	35	8	
ISO 4	10,000	2,370	1,020	352	83	
ISO 5	100,000	23,700	10,200	3,520	832	29
ISO 6	1,000,000	237,000	102,000	35,200	8,320	293
ISO 7				**352,000**	**83,200**	**2,930**
ISO 8				3,520,000	832,000	29,300
ISO 9				35,200,000	8,320,000	293,000

ISO 14644-1 to FED-STD-209E AIRBORNE PARTICULATE CLEANLINESS CLASS COMPARISON

ISO 14644-1	FED STD 209E	
1		
2		
3	1	M1.5
4	10	M2.5
5	100	M3.5
6	1,000	M4.5
7	**10,000**	**M5.5**
8	100,000	M6.5
9		

Air Sampling points for verification of ISO 14644-1, Class 7 (FED-STD-209E Class 10,000) compliance

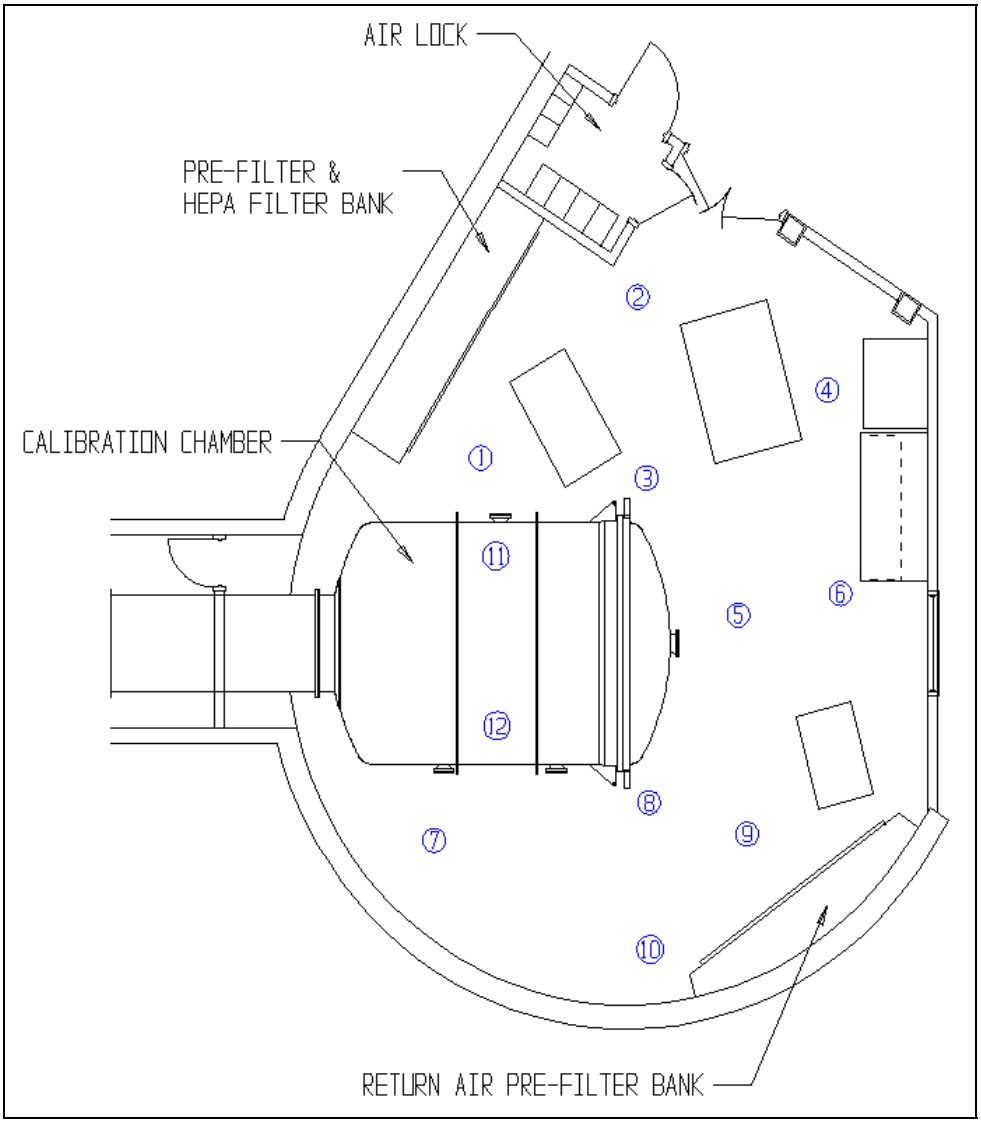

Locations to be sampled with the calibration chamber door closed:

Location Number	Lasair II Location Mnemonic
1	HEPA_LT
2	HEPA_RT
3	CHAMB_RT
4	FLOWB_LT
5	CHAMB_CTR
6	FLOWB_RT
7	BACKFILL
8	CHAMB_LT
9	PREFILT_CTR
10	PREFILT_RT

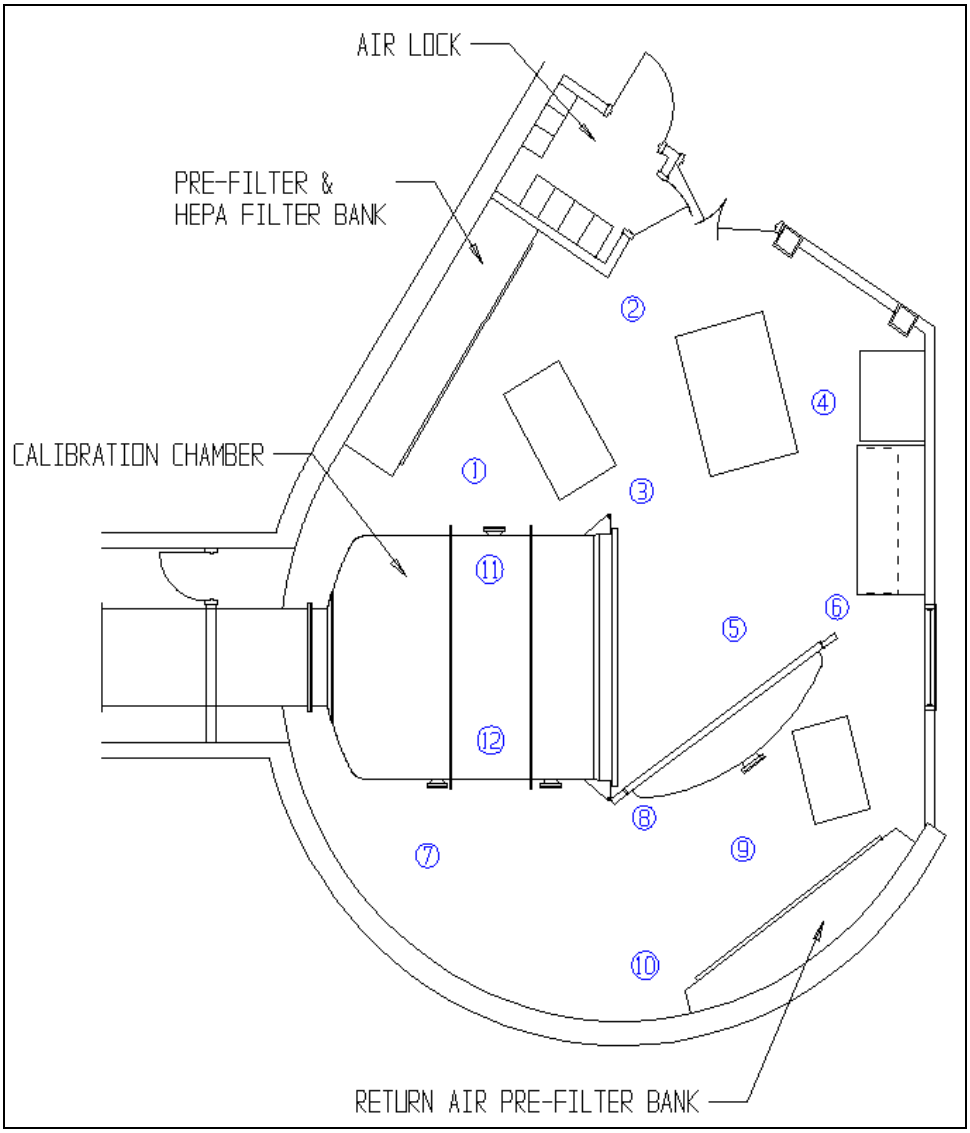

Locations to be sampled with the calibration chamber door open:

Location Number	Lasair II Location Mnemonic
1	HEPA_LT
2	HEPA_RT
3	CHAMB_RT
4	FLOWB_LT
5	CHAMB_CTR
6	FLOWB_RT
7	BACKFILL
8	CHAMB_LT
9	PREFILT_CTR
10	PREFILT_RT
11	CHAMBINT_RT
12	CHAMBINT_LT

Particle Count Data - ML 074 Cleanroom
Verification of ISO 14644-1, Class 7 (FED-STD-209E Class 10,000) Compliance
Particle Measuring Systems Lasair II Particle Counter, S/N 33657, Cal Date September 25, 2002

Zero Check

File #	Date	Time	Location	Sample Duration	Sample Size	Δ 0.3µ	Σ 0.3µ	Δ 0.5µ	Σ 0.5µ	Δ 1.0µ	Σ 1.0µ	Δ 5.0µ	Σ 5.0µ	Δ 10.0µ	Σ 10.0µ	Δ 25.0µ	Σ 25.0µ	T, °C	%RH
1	10/10/2002	17:39:00	#007	0:01:00	0.02831 m³	0	0	0	0	0	0	0	0	0	0	0	0	20.55	20.80

Chamber Door Open

File #	Date	Time	Location	Sample Duration	Sample Size	Δ 0.3µ	Σ 0.3µ	Δ 0.5µ	Σ 0.5µ	Δ 1.0µ	Σ 1.0µ	Δ 5.0µ	Σ 5.0µ	Δ 10.0µ	Σ 10.0µ	Δ 25.0µ	Σ 25.0µ	T, °C	%RH
11	10/11/2002	7:06:23	#001	0:01:00	0.02831 m³	0	0	0	0	0	0	0	0	0	0	0	0	19.86	20.70
12	10/11/2002	7:09:16	#002	0:01:00	0.02831 m³	141	141	0	0	0	0	0	0	0	0	0	0	19.86	20.70
13	10/11/2002	7:11:21	#003	0:01:00	0.02831 m³	0	0	0	0	0	0	0	0	0	0	0	0	19.96	20.61
14	10/11/2002	7:13:36	#004	0:01:00	0.02831 m³	212	212	0	0	0	0	0	0	0	0	0	0	19.86	20.61
15	10/11/2002	7:15:53	#005	0:01:00	0.02831 m³	35	71	35	35	0	0	0	0	0	0	0	0	20.06	20.51
16	10/11/2002	7:18:08	#006	0:01:00	0.02831 m³	106	106	0	0	0	0	0	0	0	0	0	0	20.06	20.51
17	10/11/2002	7:21:26	#007	0:01:00	0.02831 m³	3673	4274	459	600	141	141	0	0	0	0	0	0	20.06	20.31
18	10/11/2002	7:23:41	#008	0:01:00	0.02831 m³	565	636	35	71	35	35	0	0	0	0	0	0	20.06	20.31
19	10/11/2002	7:25:52	#009	0:01:00	0.02831 m³	35	71	0	35	35	35	0	0	0	0	0	0	20.06	20.41
20	10/11/2002	7:28:02	#010	0:01:00	0.02831 m³	3214	3567	247	353	106	106	0	0	0	0	0	0	20.06	20.61
21	10/11/2002	7:31:01	#011	0:01:00	0.02831 m³	283	494	71	212	106	141	0	35	35	35	0	0	20.06	20.51
22	10/11/2002	7:33:15	#012	0:01:00	0.02832 m³	177	247	35	71	35	35	0	0	0	0	0	0	20.06	20.41
				Mean			818		115		41		3		3		0		
				Standard Deviation			1469		187		56		10		10		0		
				S.E.			424		54		16		3		3		0		

Chamber Door Closed

File #	Date	Time	Location	Sample Duration	Sample Size	Δ 0.3µ	Σ 0.3µ	Δ 0.5µ	Σ 0.5µ	Δ 1.0µ	Σ 1.0µ	Δ 5.0µ	Σ 5.0µ	Δ 10.0µ	Σ 10.0µ	Δ 25.0µ	Σ 25.0µ	T, °C	%RH
23	10/11/2002	8:00:01	#001	0:01:00	0.02831 m³	0	0	0	0	0	0	0	0	0	0	0	0	19.57	21.09
24	10/11/2002	8:02:46	#002	0:01:00	0.02831 m³	71	177	35	106	71	71	0	0	0	0	0	0	19.67	21.09
25	10/11/2002	8:05:03	#003	0:01:00	0.02831 m³	35	35	0	0	0	0	0	0	0	0	0	0	19.67	20.90
26	10/11/2002	8:07:12	#004	0:01:00	0.02831 m³	141	141	0	0	0	0	0	0	0	0	0	0	19.67	20.80
27	10/11/2002	8:09:33	#005	0:01:00	0.02831 m³	177	353	35	177	71	141	35	71	35	35	0	0	19.86	20.80
28	10/11/2002	8:11:44	#006	0:01:00	0.02831 m³	106	141	35	35	0	0	0	0	0	0	0	0	19.96	20.61
29	10/11/2002	8:14:01	#007	0:01:00	0.02832 m³	6180	7134	565	954	353	388	0	35	35	35	0	0	20.06	20.70
30	10/11/2002	8:16:26	#008	0:01:00	0.02831 m³	0	35	35	35	0	0	0	0	0	0	0	0	20.16	20.31
31	10/11/2002	8:18:27	#009	0:01:00	0.02832 m³	35	71	35	35	0	0	0	0	0	0	0	0	20.16	20.31
32	10/11/2002	8:20:46	#010	0:01:00	0.02831 m³	3390	3638	212	247	35	35	0	0	0	0	0	0	20.16	20.41
				Mean			1173		159		64		11		7		0		
				Standard Deviation			2371		291		123		24		15		0		
				S.E.			750		92		39		8		5		0		

COR1 / NVTF Activity & Event Timeline
October 21 – December 20, 2002

Lasair 2 Sampling Episodes & Data Dumps:

1	10/10/02 to 10/25/02	Clock reset 10/17 @ 2:55pm & 4:33pm (Do not leave monitoring computer connected!)
2	10/25/02 to 11/05/02	Clock reset 10/28 @ 5:39am
3	11/05/02 to 11/20/02	Transferred to UPS power 11/08 @ 9:35am
4	11/20/02 to 12/02/02	
5	12/02/02 to 12/14/02	
6	12/17/02 to 12/30/02	Data logging failure 12/14 @ 19:35 – 12/17 @ 19:50

Activity/Event Timeline: (Times are local MDT/MST)

10/21	10:00am	Visit from BATC cleanroom contractors. Unnecessary items removed from cleanroom.
	1:00pm – 2:10pm	Move GSE into cleanroom
	2:40pm	Lasair 2 moved to CHAMBER CENTER
10/22	All day	Install nylon sleeving on all PVC cleanroom & GSE cables. Cover ESD mat on surface plate with Llumalloy to prevent Possible contamination of ETU instrument.
10/23	2:45pm	Start GSE setup & cabling in chamber
	3:15pm	Move COR1 ETU into cleanroom
	4:00pm	BATC installs NVR plates in cleanroom & chamber, installs settled particle plates in cleanroom & chamber
10/24	1:35pm	Humidity high, turn on ML070 AHU to compensate
	2:05pm	Chamber door opened Set iris to ø272mm
	4:05pm	Chamber door closed
10/25	9:40am	Chamber door opened
	10:35am	Chamber door closed for pump down
	12:20pm – 1:05pm	Install external cooling lines
	4:00pm – 4:20pm	Move UHP N2 cylinder into cleanroom
	5:05pm	Chamber @ 80mTorr, open back-fill valve
	5:40pm	Back-fill complete, open chamber door
	5:55pm	Chamber door closed
	6:05pm	Vacuum personnel entry area & airlock

10/26		Weekend – No activity
10/27		Weekend – No activity
10/28	5:35am	Chamber door clamped
	11:45am	Chamber @ 60mTorr, remove clamps, shut down pump
	12:27pm	Open back-fill valve
	1:55pm	Back-fill complete, open chamber door
	?pm	Chamber door closed
10/29	10:25am	Pull aux. vacuum pump bulkhead for tunnel entry. (focus test)
	11:30am	Enter chamber tunnel section. Install focus target.
	11:40am	Exit chamber tunnel section
	3:30pm	Enter chamber tunnel section. Remove focus target.
	3:35pm	Exit chamber tunnel section
	3:45pm	Chamber door closed
	4:00pm	Chamber door opened, install light baffling
	5:43pm	Chamber door closed
10/30		Bad Weather – No Activity
10/31		Bad Weather – No Activity
11/01		Bad Weather – No Activity
11/02		Weekend – No Activity
11/03		Weekend – No Activity
11/04	9:00am	Chamber door clamped
	9:20am	Vacuum pump started
11/05	8:45am	Coolant chiller turned on, chamber @ 40mTorr
	9:50am – 10:25am	Move two UHP N2 cylinders into cleanroom
	10:30am – 10:40am	Condensation forming on cleanroom window causing particle counter alarm to go off. Clean up water. Close & seal window cover with 2” Kapton tape.
	3:30pm	Chamber @ 60mTorr. Open back-fill valve
	4:10pm	Back-fill complete, open chamber door
	4:30pm	Chamber door closed – Polarizer Test
11/06	8:10am	Chamber @ 40mTorr
	8:30am	Chiller unit turned on
	2:10pm	Chiller unit turned off, removed chamber door clamps
	2:15pm	Chamber @ 40mTorr. Open back-fill valve

	3:00pm	Back-fill complete, open chamber door
	3:15pm	Chamber door closed – Spring Test
11/07	8:20am	Chamber @ 40mTorr, Chiller unit turned on
	2:25pm	Chamber @ 40mTorr. Open back-fill valve
	3:05pm	Back-fill complete, opened chamber door
	3:30pm	Chamber door closed
11/08	9:25am	Chamber door opened
	9:35am	Transfer Lasair II to line conditioner/UPS
	1:30pm	Install test polarizer on guider ring
	1:45pm	Chamber door closed – Polarizer Test
	1:50pm	Chamber door opened, Install Polarizer Stage on rail
	1:55pm	Chamber door closed
	2:05pm	Chamber door opened, removed polarizer from guider ring
	2:10pm	Chamber door closed for partial pump down – 100 Torr
11/09		Weekend – No Activity
11/10		Weekend – No Activity
11/11	9:05am	Back-fill from partial pump down
	9:35am	Chamber door opened
	4:25pm	Chamber door closed
11/12	7:55am	Chamber @ 40mTorr, Chiller unit turned on
	11:25am	Chamber @ 40mTorr. Open back-fill valve
	12:20pm	Back-fill complete, opened chamber door
	3:15pm	Chamber door closed
11/13	8:40am	Chamber door opened
	12:50pm	Chamber door closed
11/14	9:20am	Chamber door opened – Remove ETU electronics & cables
	11:35am	Chamber door closed
	1:00pm – 2:15pm	Drain & purge camera cooling system
	1:00pm – 1:45pm	Bill & Nelson bag GSE & Cables
	2:15pm – 2:45pm	GSE removed from cleanroom via main double door
	4:00pm	BATC rinse & sample NVR & settled particle plates, chamber & cleanroom
11/15	9:40am	Clean Llumalloy covering on surface plate
	9:50am	Chamber door opened, disconnect flex coolant lines Breadboard Instrument removed from chamber & Double bagged with Llumalloy.
	10:30am	Chamber door closed

	11:50am – 12:00am	Instrument removed from cleanroom via main double door
	12:00am – 12:20am	Cleanup & move N_2 cylinders to cleanroom door.
	4:10pm	N_2 cylinders removed from cleanroom
11/16		Weekend – No Activity, NVR & settled particle baseline
11/17		Weekend – No Activity, NVR & settled particle baseline
11/18		No Activity, NVR & settled particle baseline
11/19		No Activity, NVR & settled particle baseline
11/20		No Activity, NVR & settled particle baseline
11/21		No Activity, NVR & settled particle baseline
11/22		No Activity, NVR & settled particle baseline
11/23		Weekend – No Activity, NVR & settled particle baseline
11/24		Weekend – No Activity, NVR & settled particle baseline
11/25		No Activity, NVR & settled particle baseline
11/26		No Activity, NVR & settled particle baseline
11/27		No Activity, NVR & settled particle baseline
11/28		No Activity, NVR & settled particle baseline
11/29		No Activity, NVR & settled particle baseline
11/30		Weekend – No Activity, NVR & settled particle baseline
12/01		Weekend – No Activity, NVR & settled particle baseline
12/02		No Activity, NVR & settled particle baseline
12/03		No Activity, NVR & settled particle baseline
12/04		No Activity, NVR & settled particle baseline
12/05		No Activity, NVR & settled particle baseline
12/06		No Activity, NVR & settled particle baseline

12/07		Weekend – No Activity, NVR & settled particle baseline
12/08		Weekend – No Activity, NVR & settled particle baseline
12/09		No Activity, NVR & settled particle baseline
12/10		No Activity, NVR & settled particle baseline
12/11		No Activity, NVR & settled particle baseline
12/12		No Activity, NVR & settled particle baseline
12/13		No Activity, NVR & settled particle baseline
12/14		Weekend – No Activity, NVR & settled particle baseline
12/15		Weekend – No Activity, NVR & settled particle baseline
12/16		No Activity, NVR & settled particle baseline
12/17		No Activity, NVR & settled particle baseline
12/18		No Activity, NVR & settled particle baseline
12/19		No Activity, NVR & settled particle baseline
12/20		No Activity, NVR & settled particle baseline
	4:00pm	BATC rinse & sample NVR & settled particle plates, chamber & cleanroom